Hydrogen bonding in the benzene–ammonia dimer

David A. Rodham*, Sakae Suzuki*, Richard D. Suenram†, Frank J. Lovas†, Siddharth Dasgupta‡, William A. Goddard III‡ & Geoffrey A. Blake§

* Division of Chemistry and Chemical Engineering, 127-72, California Institute of Technology, Pasadena, California 91125, USA
† Molecular Physics Division, National Institute of Standards and Technology, Gaithersburg, Maryland 20899, USA
‡ Materials and Molecular Simulation Center, Beckman Institute, 139-74, California Institute of Technology, Pasadena, California 91125, USA
§ Division of Geological and Planetary Sciences, 170-25, California Institute of Technology, Pasadena, California 91125, USA

AMINES have long been characterized as amphoteric (acting as both donor and acceptor) in terms of their hydrogen-bond interactions in the condensed phase. With the possible exception of $(NH_3)_2$, however, no gas-phase complexes exhibiting hydrogen-bond donation by ammonia, the 'simplest amine', have been observed[1,2]. Here we present high-resolution optical and microwave spectra of the benzene–ammonia dimer in the gas phase, which show that the ammonia molecule resides above the benzene plane and undergoes free or nearly free internal rotation. In the vibrationally averaged structure, the C_3 symmetry axis of NH_3 is tilted by about 58° relative to the benzene C_6 axis, such that the ammonia protons interact with the benzene π-cloud. Our *ab initio* calculations predict a 'monodentate' minimum-energy structure, with very low barriers to rotation of ammonia. The larger separation of the two molecular components, and the smaller dissociation energy, relative to the benzene–water dimer[3] reflect the weak hydrogen-bond donor capability of ammonia, but the observed geometry greatly resembles the amino–aromatic interaction found naturally in proteins[4].

Typically, hydrogen-bond interactions have energies of 8–29 kJ mol^{-1} (2–7 kcal mol^{-1}) and are thought to involve essentially linear arrangements of donors, such as -OH or -NH groups, with a proton acceptor, often a highly electronegative atom. From this 'classical' point of view, the interactions of hydrogen-bond donors with aromatic systems are of both theoretical and practical interest as they can be used to probe the general limits of hydrogen-bonding functional groups[5]. The amino-aromatic and ammonium-aromatic interactions are common motifs in protein structure and in rational molecular design[4,6]. Crystallographic imaging of specific interactions, such as that in the binding region of the *v-src* SH2 domain[7], is consistent with 'hydrogen-bond' donation from the $-NH_2$ and $-NH_3^+$ groups, although the *in vivo* stability of such structures is difficult to estimate[8].

In principle, the energetics and structural parameters of the amino-aromatic interaction, free of external perturbations, may be derived from isolated weakly bound clusters. The simplest of these would be the benzene-ammonia dimer. But gas-phase ammonia can best be described as a powerful proton acceptor[1]. In recent work on C_6H_6-H_2O (ref. 3), we found that benzene does act as a 'hydrogen-bond' acceptor in this complex. Given the similarity of the observed structure to analogous hydroxyl-aromatic and amino-aromatic interactions found in proteins, we started the present study on the benzene-ammonia dimer.

We have used resonance-enhanced two-photon ionization (R2PI) and microwave spectroscopy along with quantum chemical calculations to study the structure and energetics of the C_6H_6-NH_3 system. Ionization is enhanced when the energy of the ionizing laser is in resonance with a rovibronic transition of the cluster. The fine structure of the resonances provides insights into the rotational dynamics of the cluster, and thus on the bonding geometry. Typical R2PI spectra through the $S_1 \leftarrow S_0(6_0^1)$ transition of benzene are shown in Fig. 1. Results for ND_3 mixtures were similar. Features assigned to the dimer remained at low ammonia concentrations (0.01%), and were the only peaks for which cluster fragmentation produced significant numbers of free benzene cations. Most of the other spectral features in Fig. 1*a* resulted from the efficient fragmentation of larger clusters after ionization. Earlier R2PI spectra of C_6H_6-NH_3 were extremely complex because of such fragmentation[9], which provides indirect evidence for a hydrogen-bonded geometry[10].

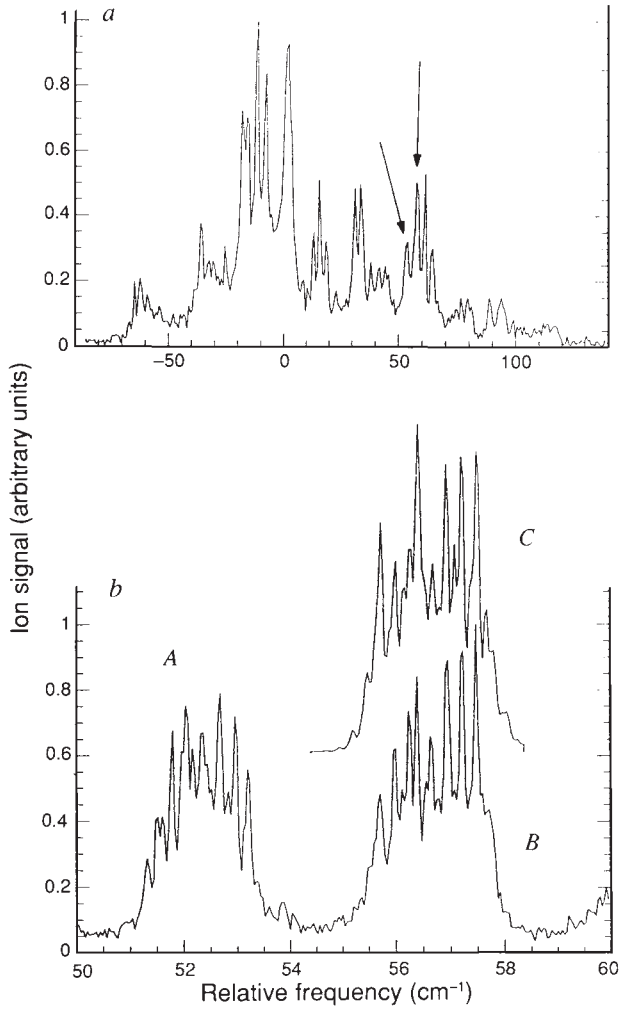

FIG. 1 R2PI spectra of C_6H_6-NH_3, obtained by ionizing clusters in a skimmed molecular beam with the frequency-doubled output of an excimer-pumped dye laser in the source region of a reflection time-of-flight mass spectrometer. *a*, Low-resolution spectrum (0.4 cm^{-1} laser bandwidth, 0.75 cm^{-1} per point) recorded by monitoring the $[C_6H_6$-$NH_3]^+$ mass channel at high NH_3 concentration (0.27%). The frequency scale is relative to the 6_0^1 transition of free benzene. Arrows point to the 6_0^1 transition of the 1:1 complex; most of the other features are fragmentation products of larger clusters. *b*, Higher-resolution (0.08 cm^{-1} laser bandwidth, 0.04 cm^{-1} per point) scan of the 1:1 complex 6_0^1 band. *A* is assigned to an excited $m=1$ internal rotor state, *B* originates from the ground $m=0$ internal rotor state, and *C* is a calculated fit of the $m=0$ band. For this case of a symmetric top with a free internal rotor, the *A* rotational constants for the S_0 and S_1 electronic states of the complex should be close to the *c*-axis constants of free benzene, as is observed. Using the free rotor (benzene *c*-axis) values of $A''=0.0948$ cm^{-1} and $A'=0.0906$ cm^{-1} plus the B'' ground state rotational constants from Table 1, the best fits produced $B'=0.0640$ cm^{-1}, $\zeta=-0.48$ for C_6H_6-NH_3 and $B'=0.0578$ cm^{-1}, $\zeta=-0.58$ for C_6H_6-ND_3. The benzene $S_1(6^1)$ Coriolis parameter is $\zeta=-0.58$, and the highest correlation in the fits is between A' and ζ.

High-resolution R2PI scans (Fig. 1*b*) demonstrate that the

TABLE 1 Spectroscopic fits to $m=0$ microwave data

Complex	B(MHz)	D_J(kHz)	D_{JK}(kHz)	σ(MHz)	
C_6H_6-$^{14}NH_3$	1,889.026 (3)	4.03 (4)	91.52 (9)	0.038	$eQq_{aa}=0.286$ (15) MHz
C_6H_6-$^{15}NH_3$	1,830.4272 (7)	3.87 (3)	89.50 (6)	0.003	$\mu_a=3.814(15)\times10^{-1}$ cm
C_6H_6-$^{14}ND_3$	1,732.986 (7)	3.77 (3)	127.79 (51)	0.030	(1.142 (5) D)

Spectra of the $J=6\leftarrow5$ and $J=7\leftarrow6$ transitions of C_6H_6-$^{14}NH_3$ were initially recorded using the Stark modulation microwave absorption spectrometer at the California Institute of Technology. Clusters were formed by expanding Ar seeded with ~1% of both C_6H_6 and NH_3 through a 50 mm × 0.025 mm slit nozzle. Spectra of the $J=3\leftarrow2$ and $4\leftarrow3$ transitions of benzene complexed with $^{14}NH_3$, $^{15}NH_3$ and $^{14}ND_3$ were subsequently obtained with the Fourier transform microwave spectrometer at NIST-Gaithersburg. Both instruments have been described in detail previously[17,18]. Transition frequencies were fitted using the standard symmetric-top equation $\nu(J\rightarrow J-1)=2J(B-D_{JK}K^2)-4D_JJ^3$, where B is the rotational constant and D_J and D_{JK} are the 'stretching' and 'bending' centrifugal distortion constants of the dimer. σ Is the root-mean-square error of the fit. Dipole moments for the -$^{14}NH_3$ and -$^{15}NH_3$ complexes were determined from the Stark shifts of the $K=0$ lines in a static electric field, and are the same within experimental error. The $J=3\leftarrow2$, $K=2$ transition was used to determine the quadrupole moment of C_6H_6-$^{14}NH_3$. From these measurements, the angular projections were calculated in the standard fashion: $\mu_a(C_6H_6\text{-}NH_3)=\mu_{ind}+\mu_{NH_3}\langle\cos\theta\rangle$; $eQq_{aa}(C_6H_6\text{-}NH_3)=eqQ_{NH_3}\langle[3\cos^2\theta-1]/2\rangle$. The measured $P_2(\cos\theta)$ and μ_a values produce a μ_{ind} of 1.0×10^{-30} C m (0.3 Debye units, D), which is consistent with estimates based on the ammonia dipole moment and the polarizability of benzene when $\langle\theta\rangle\sim60°$. The *ab initio* calculations find $\theta^e=52°$, $\mu(NH_3)=5.67\times10^{-30}$ C m (1.89 D), and μ_a (C_6H_6-NH_3) $=4.32\times10^{-30}$ C m (1.44 D), which yield μ_{ind}(MP2/6-31G**) $=1.0\times10^{-30}$ C m (0.3 D).

dimer retains symmetry about the benzene C_6 axis on a vibrationally averaged basis. The appearance of two peaks suggests that the ammonia can freely rotate in C_6H_6-NH_3, with one band arising from the $[j(NH_3)=0, m=0]$ ground state and the other from the $[j(NH_3)=1, m=1]$ internal rotor state. The $m=1$ states are metastable because of nuclear spin eigenfunction restrictions[10]. A least-squares fit to the $m=0$ band using nuclear spin statistical weights determined for the G_{36} molecular symmetry group is shown in Fig. 1*b* (trace C). The G_{36} group considers the internal rotation of the monomers and the exchange of the ammonia protons, but not inversion, to be 'feasible'. The shape of the $m=0$ contour is sensitive to the A rotational constant of the dimer and is consistent only with a symmetric structure in which a nearly freely internally rotating ammonia resides above the benzene plane, suggesting the general structure shown in Fig. 2. Ammonia inversion may well occur in C_6H_6-NH_3, but the R2PI data show no direct evidence of it.

These conclusions are strengthened by the symmetric-top pure rotational (microwave) spectra observed for the $m=0$ state (data available from the authors on request). Transitions originating from the $m=1$ states have not yet been observed in the microwave region, but they are not critical to the structural determination outlined below. The rotational and centrifugal distortion constants for three isotopic species (C_6H_6-$^{14}NH_3$, -$^{15}NH_3$, -$^{14}ND_3$) obtained from the $m=0$ data are listed in Table 1. The rotational constants are consistent with the structure deduced from the R2PI data, as is outlined in Fig. 2. A Lennard-Jones approximation to the radial potential and the centrifugal distortion constant D_J in Table 1 lead to an experimental estimate of ~5.9 kJ mol^{-1} (1.4 kcal mol^{-1}) for the zero-point dissociation energy D_0 and a stretching force constant of 4.1(2) N m^{-1}. The slight decrease and large increase in the values of the distortion constant D_{JK} on isotopic substitution of -$^{15}NH_3$ and -ND_3 are predicted to within 20% by a harmonic bending potential, which yields a bending force constant of 1–2 N m^{-1}.

This same general structure has been found for the C_6H_6-HCl (ref. 11), C_6H_6-HF (ref. 12), and C_6H_6-H_2O (refs 3, 10) hydrogen-bonded complexes. These dimers, like C_6H_6-NH_3, exhibit symmetric-top ground-state spectra as a result of internal rotation or vibrational averaging that maintains symmetry about the benzene C_6 axis. In addition to the rotational constants, the *a*-axis projection of the nitrogen nuclear quadrupole coupling constant (eQq_{aa}) and electric dipole (μ) moments of the cluster were measured and used to extract NH_3 $P_2(\theta)$ and $P_1(\theta)$ angular projections. The NH_3 tilt angle determined from eQq_{aa} is $\langle\theta^2\rangle^{1/2}=57.6\pm0.3°$. Uncertainties in the induced dipole (μ_{ind}) moment render the $P_1(\theta)$ value more suspect, but for a range of $\pm0.33\times10^{-30}$ cm (±0.1 Debye unit (D)) in μ_{ind} we estimate that $\langle\theta\rangle=60\pm5°$ (see Table 1). The consistency of the angular expectation values, in contrast to those observed for Ar-NH_3 and Ar-H_2O (ref. 13), clearly indicate that the ammonia protons

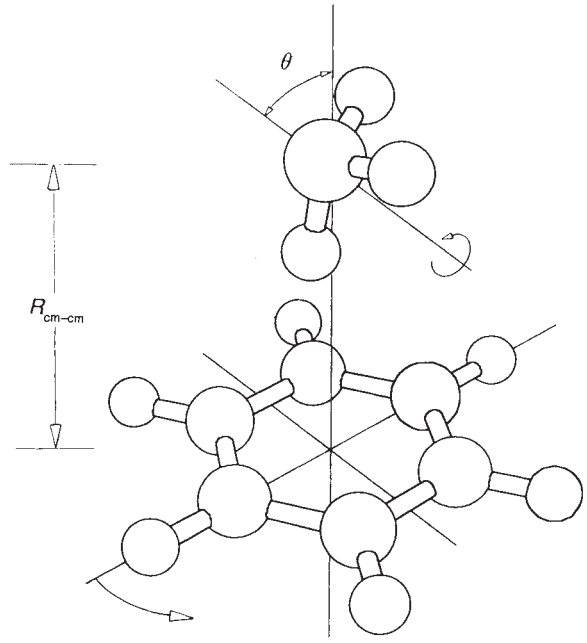

FIG. 2 Coordinate system and structure of the benzene–ammonia dimer. To calculate the weak bond length and the tilt angle of the ammonia, we used the formula[19]

$$I_{bb(C_6H_6\text{-}NH_3)}=\mu R^2_{(cm-cm)}+\frac{I_{bb(NH_3)}}{2}\langle1+\cos^2\theta\rangle+\frac{I_{cc(NH_3)}}{2}\langle\sin^2\theta\rangle+I_{bb(C_6H_6)}$$

where θ is the angle between the NH_3 C_3 axis and the benzene C_6 axis, with the ammonia centre of mass on the benzene C_6 axis and $\theta=0$ corresponding to the configuration in which all three ammonia protons point toward the benzene. μ is the pseudodiatomic reduced mass of the complex and $R_{(cm-cm)}$ is the distance between the molecular centres of mass. $I_{cc}(NH_3)$ and $I_{bb}(NH_3)$ are the ammonia moments of inertia parallel and perpendicular to the ammonia C_3 symmetry axis. Arrows depict the feasible large amplitude motions in this complex. Assuming that the distance from the nitrogen atom to the benzene plane $R_{N\text{-}Bz}$ was the same for all three isotopic species led to independent constraints on $R_{N\text{-}Bz}$ and θ, which were found to be $R_{N\text{-}Bz}=3.590\pm0.005$ Å and $\theta=59\pm5°$. The above equation assumes that the vibrational averaging of the benzene orientation is negligible. Tilting of the benzene plane by 5 and 10° reduces the $R_{N\text{-}Bz}$ by 0.0035 and 0.015 Å, respectively. Because of the symmetric top character of the monomers, the individual ammonia proton locations cannot be determined experimentally.

are 'bound' to the benzene π-cloud: that is, the anisotropy in the intermolecular potential is substantial.

To estimate the binding energy and other global properties of the intermolecular potential, theoretical calculations were performed for the dimer using the program Gaussian 92 (ref. 14) at the MP2/6-31G** level. Previous *ab initio* efforts on this complex have either neglected electron correlation[15] or not used it in scans of the potential energy surface[16], but show, as here, that the binding well is shallow. The MP2/6-31G** non-BSSE (non-basis set superposition error-corrected) binding energy is $D_e \approx 10$ kJ mol^{-1} (2.4 kcal mol^{-1}). Full energy minimization of the intermolecular degrees of freedom produced an equilibrium structure ($R^e_{cm-cm} = 3.43$ Å, $\theta^e = 52°$) which is very similar to that experimentally observed, but different from that predicted solely from the leading electrostatic attractive forces (dipole-induced dipole, dipole-quadrupole and so on). The calculations indicate that the geometry where one proton is pointing towards the centre of the benzene ring is slightly more stable than that with two protons pointing towards the benzene ring. In both minima the ammonia centre of mass lies above the plane of benzene along its C_6 axis. The energy difference between the 'monodentate' and 'bidentate' geometry, however, is only 0.4 kJ mol^{-1} (0.1 kcal mol^{-1}), a value comparable to the intermolecular zero-point vibrational energies.

The predicted D_e is at the lowest end of the range commonly accepted for hydrogen bonding—the hydrogen-bond energy in water ice is near 21 kJ mol^{-1} (5 kcal mol^{-1}), and typical O-H · · · O and N-H · · · N hydrogen bonds range in strength from 13–25 to 8–21 kJ mol^{-1} (3–6 to 2–5 kcal mol^{-1}; ref. 5)—and is considerably below that of C_6H_6–H_2O (ref. 3), consistent with the gas-phase acidities of ammonia and water. Nevertheless, the benzene–ammonia dimer constitutes a rare example of proton donation by ammonia in weakly bound complexes, and provides the simplest molecular model of the biologically important amino–aromatic interaction. □

Received 11 January; accepted 9 March 1993.

1. Nelson, D. D. Jr, Fraser, G. T. & Klemperer, W. *Science* **238,** 1670–1674 (1987).
2. Loeser, J. G. *et al. J. chem. Phys.* **97,** 4727–4749 (1992).
3. Suzuki, S. *et al. Science* **257,** 942–945 (1992).
4. Burley, S. K. & Petsko, G. A. *FEBS Lett.* **203,** 139–143 (1986).
5. Pimental, G. C. & McClellan, A. L. *The Hydrogen Bond,* 202–203 (Freeman, San Francisco, 1960).
6. Dougherty, D. & Stauffer, D. A. *Science* **250,** 1558–1560 (1990).
7. Waksman, G. *et al. Nature* **358,** 646–653 (1992).
8. Perutz, M. F. in *The Chemical Bond* (ed. Zewail, A.) 17–30 (Academic, New York, 1992).
9. Wanna, J., Menapace, J. A. & Bernstein, E. R. *J. chem. Phys.* **85,** 1795–1805 (1986).
10. Gotch, A. J. & Zwier, T. S. *J. chem. Phys.* **96,** 3388–3401 (1992).
11. Read, W. G., Campbell, E. J. & Henderson, G. *J. chem. Phys.* **78,** 3501–3508.
12. Baiocchi, F. A., Williams, J. H. & Klemperer, W. *J. phys. Chem.* **87,** 2079–2084 (1983).
13. Cohen, R. C. & Saykally, R. J. *J. phys. Chem.* **96,** 1024–1040 (1992).
14. Fritsch, M. J. *et al. Gaussian 92* (Gaussian, Pittsburgh, PA, 1992).
15. Cheney, B. V., Schulz, M. W., Cheney, J. & Richards, W. G. *J. Am. chem. Soc.* **110,** 4195–4198 (1988).
16. Bredas, J. L. & Street, G. B. *J. chem. Phys.* **90,** 7291–7299 (1989).
17. Bumgarner, R. E. & Blake, G. A. *Chem. Phys. Lett.* **161,** 308–314 (1989).
18. Suenram, R. D. *et al. J. molec. Spectrosc.* **137,** 127–137 (1989).
19. Fraser, G. T., Lovas, F. J., Suenram, R. D., Nelson, D. D. & Klemperer, W. *J. chem. Phys.* **84,** 5983–5988 (1986).

ACKNOWLEDGEMENTS. We gratefully acknowledge support from the Caltech Beckman Institute (to W.A.G.), NSF, NASA and the David and Lucille Packard Foundation (to G.A.B.).

Seasonal and diel variation in the open ocean concentration of marine snow aggregates

R. S. Lampitt, W. R. Hillier & P. G. Challenor

Institute of Oceanographic Sciences Deacon Laboratory, Wormley, Godalming, Surrey GU8 5UB, UK

MARINE snow, generally defined as aggregated particles of diameter greater than 0.5 mm, is thought to play an important role in oceanic biogeochemical cycles[1]. Recent studies have focused on its unusual physical, biological and chemical properties but its temporal variability has received scant attention[2–6]. Here we report observations of the abundance, volume concentration and size distribution of marine snow over a five-month period at a single site in the Northeast Atlantic. At a depth of 270 m, marine snow particles demonstrated strong seasonal and diel variability. Volume concentrations in spring were about 20 times those in summer and autumn with late morning concentrations up to three times higher than at other times of the day. Our results suggest that the marine snow forms as a result of highly dynamic interactions in the particle pool. We believe that the mid-water biota and their migratory behaviour are responsible for the diel variability; they are therefore likely to have a significant influence on marine snow concentrations and hence on open-ocean material flux.

A camera system was deployed on a mooring above the Porcupine abyssal plain in the mesotrophic Northeast Atlantic (47° 45′ N, 19° 28′ W) on 20 April 1990 and recovered 154 days later after taking images of a 20-litre volume every 512 minutes. The apparatus was at an average depth of 270 m. After image processing and data analyses, a strong seasonal signal became apparent. In addition, contrary to expectations, both abundance and volume concentration of marine snow tended to be higher in the day than at night (Fig. 1). Two main abundance and concentration peaks occurred (mid-April and mid to late May). The initial rapid increases in volume concentration were mainly because of increased abundance of the larger particles (>2.5 mm diameter) but later within the peaks, the volume was dominated by the smaller size categories (1.6–2.5 mm) (Fig. 2). The smallest size categories vary only slowly during the year, presumably reflecting their longer residence time in the water column.

Large changes in the particle pool sometimes occurred over short time periods (less than a day) causing 10-fold changes in volume concentration and threefold changes in abundance. A variety of explanations may be offered for these observations, the simplest of which is the advection of water masses with different particle characteristics. Variation in temperature, current speed or direction recorded 80 m above the camera were not correlated with changes in marine snow concentration, although there were substantial long-term changes in current direction and speed. Furthermore if the observed particles sink at rates of ~100 m d^{-1} (refs 7, 8), they would have been produced in the upper mixed layer within 100 km of the mooring even at the highest current speeds recorded. The temporal changes can thus be considered as representative of this particular oceanographic regime.

Knowledge of the concentration of marine snow in the world's oceans is sparse and is based on a small number of observations[1–6]. Most of these observations were made in the Pacific and generally report only the abundance, a parameter which is very sensitive to the lower size limit of the recording system. Nevertheless the absolute values of abundance and volume concentration found here in the summer and autumn at 270 m are very similar to two recent records from the western Atlantic[5], implying agreement between different techniques in similar environments. Previous reports may well have missed pulses of marine snow because they lacked temporal coverage, and conclusions drawn from them should be treated with caution.

We believe that the observed variability reflects changes over time in the hydrographic and biological processes in the upper water column that are responsible for the production of marine snow. The Northeast Atlantic is an area of intense seasonality, and the seasonal marine snow signal clearly reflects trends in